Supplementary Information for: Disentangling Coexisting Structural Order Through Phase Lock-in Analysis of Atomic-Resolution STEM Data

Berit H. Goodge[1], Ismail El Baggari[2], Sung Sae Hong[3,4], Zhe Wang[1], Darrell G. Schlom[5,6], Harold Y. Hwang[3,4], & Lena F. Kourkoutis[1,6]

[1]*School of Applied and Engineering Physics, Cornell University, Ithaca, NY 14853, USA*

[2]*Department of Physics, Cornell University, Ithaca, NY 14853, USA*

[3]*Geballe Laboratory for Advanced Materials, Stanford University, Stanford, California 94305, USA*

[4]*Stanford Institute for Materials and Energy Sciences, SLAC National Accelerator Laboratory, Menlo Park, California 94025, USA*

[5]*Department of Materials Science and Engineering, Cornell University, Ithaca, NY, 14853-1501 USA*

[6]*Kavli Institute at Cornell for Nanoscale Science, Cornell University, Ithaca, NY 14853, USA*

† *current address: Rowland Institute at Harvard, Cambridge, MA 02142, USA*

‡ *current address: Department of Materials Science and Engineering, University of California Davis, Davis, CA 95616, USA*

Correspondence to:

Lena F. Kourkoutis
School of Applied and Engineering Physics
Cornell University
142 Sciences Dr.
Ithaca, NY 14853
phone: (607) 255-9121
fax: 607 255-7658
email: lena.f.kourkoutis@cornell.edu

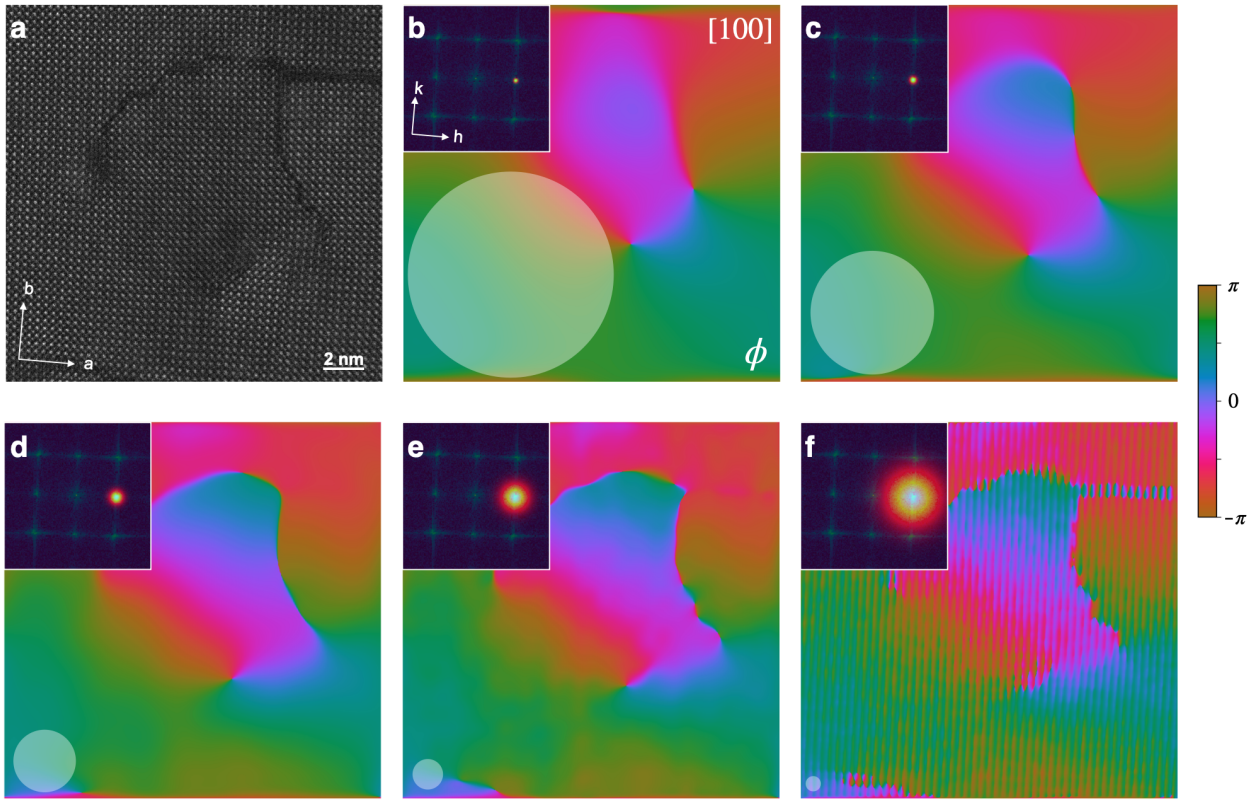

Figure S1: Effect of Gaussian Fourier mask size on the coarse-graining in the resulting phase map. (a) HAADF-STEM image of the extended defect shown in main text Figure 2. (b)-(f) Phase lock-in analysis generated phase maps of the [100] Bragg peak (see main text Figure 2b) with different mask sizes as shown in the inset FFTs. The real-space coarsening length of each mask size is shown by the white circle in the bottom-left corner of each phase map. Small mask sizes lead to large coarsening lengths, which reduces the sensitivity of the technique to different lattice defects, as seen in (b) and (c). When the mask size is too large, the technique is overly sensitive to frequencies near that of the lattice, and artefacts such as the fringing observed in (f) begin to emerge.

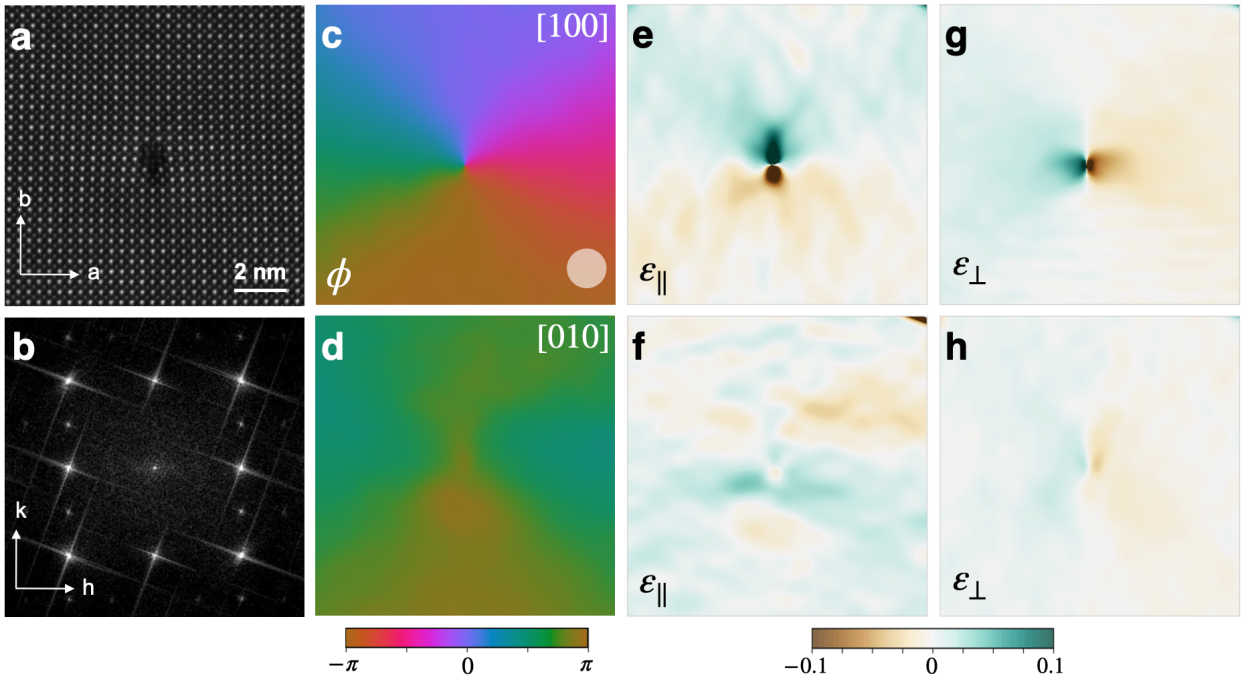

Figure S2: Raw phase and strain maps for the phase lock-in analysis of a simple edge dislocation shown in Figure 1 of the main text. The circle in (c) shows the real-space coarsening length of the lock-in analysis in all maps.

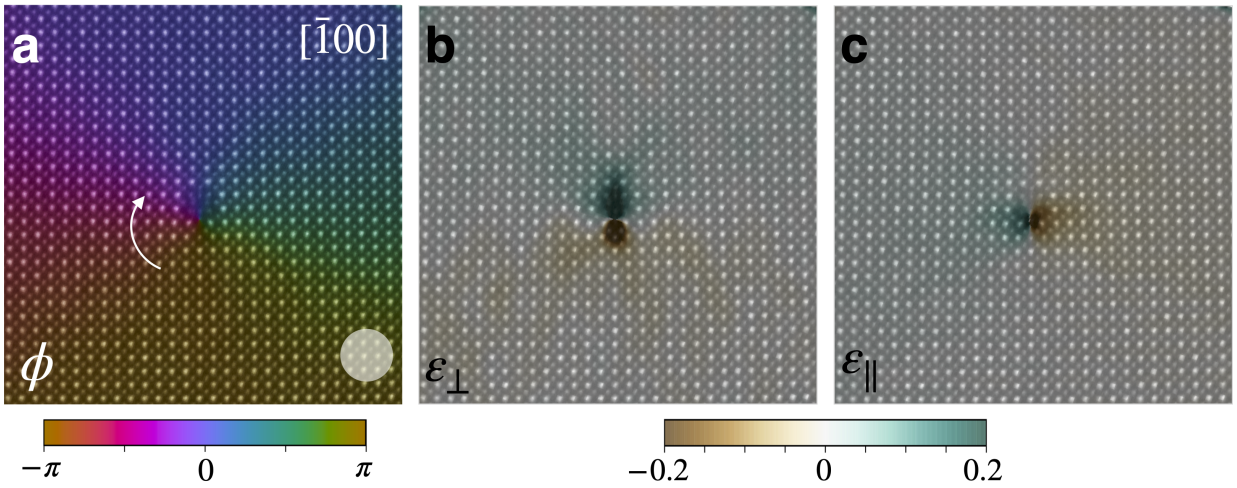

Figure S3: Phase lock-in analysis of the symmetric [$\bar{1}$00] peak for the same edge dislocation shown in Figure 1 of the main text. The resulting phase map is identical but inverted, with the direction of the 2π phase winding reversed (marked by the white arrow). Note that the resulting strain maps are exactly identical because both the phase and the wavevector are reversed. The circle in (c) shows the real-space coarsening length of the lock-in analysis in all maps. The circle in (a) shows the real-space coarsening length of the lock-in analysis in all maps.

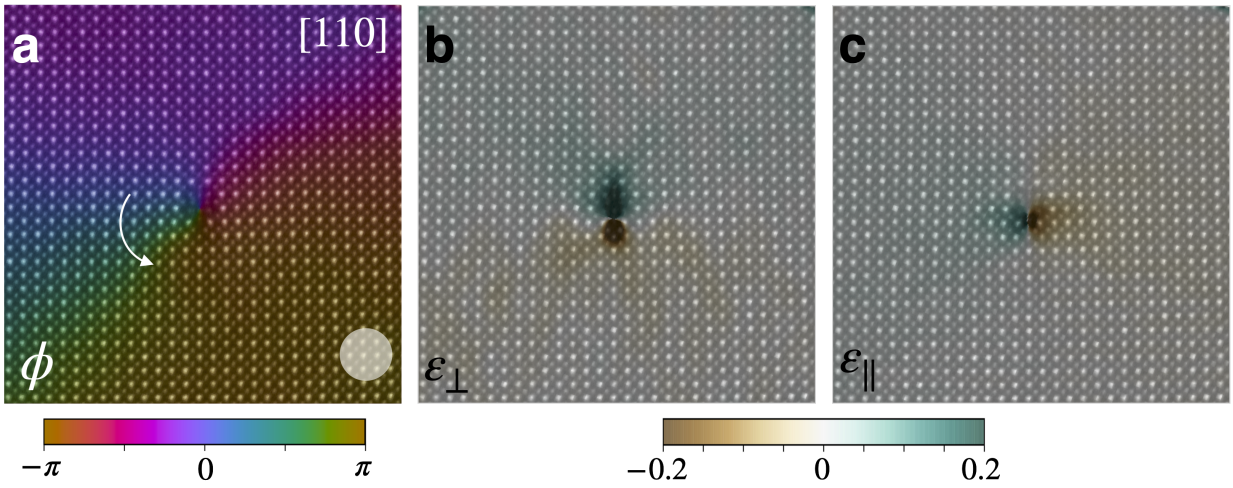

Figure S4: Phase lock-in analysis of the intermediate [110] peak for the same edge dislocation shown in Figure 1 of the main text. The 2π phase winding and strain singularities revealed by analysis of the [100] peak can be observed, but distorted by the skew resulting from a projection of $\vec{b} = [100]$ onto $\vec{q} = [110]$. The circle in (a) shows the real-space coarsening length of the lock-in analysis in all maps.